

# Comparative analysis of zinc-blende and wurtzite GaN for full-band polar optical phonon scattering and negative differential conductivity

C. Bulutay, B. K. Ridley, and N. A. Zakhleniuk

Citation: *Appl. Phys. Lett.* **77**, 2707 (2000); doi: 10.1063/1.1320020

View online: <https://doi.org/10.1063/1.1320020>

View Table of Contents: <http://aip.scitation.org/toc/apl/77/17>

Published by the [American Institute of Physics](#)

---

## Articles you may be interested in

[Transition between wurtzite and zinc-blende GaN: An effect of deposition condition of molecular-beam epitaxy](#)  
*Applied Physics Letters* **89**, 151921 (2006); 10.1063/1.2360916

[Comparison of zinc-blende and wurtzite GaN semiconductors with spontaneous polarization and piezoelectric field effects](#)  
*Journal of Applied Physics* **87**, 353 (2000); 10.1063/1.371915

[Electronic transport studies of bulk zincblende and wurtzite phases of GaN based on an ensemble Monte Carlo calculation including a full zone band structure](#)  
*Journal of Applied Physics* **78**, 1033 (1995); 10.1063/1.360405

[Electronic band structures and effective-mass parameters of wurtzite GaN and InN](#)  
*Journal of Applied Physics* **83**, 1429 (1998); 10.1063/1.366847

[Band gap engineering of wurtzite and zinc-blende GaN/AlN superlattices from first principles](#)  
*Journal of Applied Physics* **108**, 103701 (2010); 10.1063/1.3505752

[Deep traps in AlGaIn/GaN heterostructures studied by deep level transient spectroscopy: Effect of carbon concentration in GaN buffer layers](#)  
*Journal of Applied Physics* **108**, 063706 (2010); 10.1063/1.3488610

---



The image shows a Lake Shore Measure Ready 155 Precision I/V Source. The device is a rectangular, silver-colored unit with a black front panel. On the left side, there is a color LCD screen displaying 'AC Peak Amplitude 10.000 mV', 'Frequency 100.000 kHz', and 'DC Offset 0.0000 mV'. To the right of the screen are several control buttons and a rotary switch. On the right side of the front panel, there are two sets of terminals labeled 'CURRENT' and 'VOLTAGE'. The Lake Shore logo is visible in the top left corner of the device's front panel. The background of the advertisement is dark blue.

**Lake Shore**  
CRYOTRONICS

**Measure Ready**  
**155 Precision I/V Source**

A new current & voltage source  
optimized for scientific research

**LEARN MORE** ▶

# Comparative analysis of zinc-blende and wurtzite GaN for full-band polar optical phonon scattering and negative differential conductivity

C. Bulutay<sup>a)</sup> and B. K. Ridley

*Department of Electronic Systems Engineering, University of Essex, Colchester CO4 3SQ, United Kingdom*

N. A. Zakhleniuk

*Caswell Technology, Marconi Caswell, Towcester, Northants, NN12 8EQ, United Kingdom*

(Received 26 May 2000; accepted for publication 1 September 2000)

For high-power electronics applications, GaN is a promising semiconductor. Under high electric fields, electrons can reach very high energies where polar optical phonon (POP) emission is the dominant scattering mechanism. So, we undertake a full-band analysis of POP scattering of conduction-band electrons based on an empirical pseudopotential band structure. To uncover the directional variations, we compute POP emission rates along high-symmetry directions for the zinc-blende (ZB) crystal phase of GaN. We also compare the results with those of the wurtzite phase. In general, the POP scattering rates in the zinc-blende phase are lower than the wurtzite phase. Our analysis also reveals appreciable directional dependence, with the  $\Gamma-L$  direction of ZB GaN being least vulnerable to POP scattering, characterized by a scattering time of 11 fs. For both crystal phases, we consider the negative differential conductivity possibilities driven by the negative effective mass part of the band structure. According to our estimation, for the ZB phase the onset of this effect requires fields above  $\sim 1$  MV/cm. © 2000 American Institute of Physics.

[S0003-6951(00)02743-1]

The wide-band-gap III-nitride semiconductors are currently being considered for high-power and high-temperature applications. Among these III nitrides, the most studied is GaN which can be grown either in wurtzite (WZ) or zinc-blende (ZB) phases depending on the choice of the substrate and the growth conditions.<sup>1</sup> The mounting interest in the high-field applications of GaN, brings under demand a detailed knowledge of the transport properties, like the characterization of the dominant scattering mechanism. This, in GaN is the polar optical phonon (POP) scattering due to its high degree of ionicity.<sup>2</sup> A realistic high-field analysis inevitably requires a full-band treatment as the carriers under the influence of such high fields move further away from the band edge where their scattering rate depends on the details of the band structure.

In this letter, we present a full-band analysis of the POP scattering of conduction-band (CB) electrons based on the empirical pseudopotential band structure. To shed light on the effects of the crystal phase, we consider both ZB and WZ structures. We place more emphasis on the ZB phase, as a comprehensive discussion of the WZ case has been given by us elsewhere.<sup>3</sup> For the empirical pseudopotential band structure of ZB GaN, we use published form factors,<sup>4</sup> however, for the case of WZ GaN we felt the necessity to develop our own form factors<sup>3</sup> due to the poor performance of the CB properties of the available ones.

Considering the ZB case, the scattering rate based on Fermi's Golden Rule due to POP emission of an electron at the band  $m$ , with a wave vector  $\mathbf{k}$ , is given by

$$W_m(\mathbf{k}) = \frac{2\pi}{\hbar} \frac{V}{(2\pi)^3} \sum_{m'} \int_{1st\ BZ} d^3k' \Delta_{m',m}(\mathbf{k}', \mathbf{k}) \times |C_{POP}(q)|^2 \delta(E_{m'}(\mathbf{k}') - E_m(\mathbf{k}) + \hbar\omega_{LO}), \quad (1)$$

where the emitted phonon wave vector is  $\mathbf{q} = -\mathbf{k}' + \mathbf{k}$  mapped to first BZ, the primed indices represent final-state electron labels over which a summation/integration is performed,  $V$  is the total crystal volume,  $E_m(\mathbf{k})$  is the band energy of the electron, and  $\hbar\omega_{LO}$  is the longitudinal-optical (LO) phonon energy assumed to be dispersionless. The cubic POP coupling constant is given by  $|C_{POP}(q)|^2 = 2\pi e^2 \hbar\omega_{LO} (\epsilon_\infty^{-1} - \epsilon_0^{-1}) / (Vq^2)$ , where  $\epsilon_0$  and  $\epsilon_\infty$  are the static and high-frequency dielectric constants. The cell-periodic overlap parameter is given by  $\Delta_{m',m}(\mathbf{k}', \mathbf{k}) = |(1/\Omega) \int_\Omega u_{m',\mathbf{k}'}^*(\mathbf{r}) u_{m,\mathbf{k}}(\mathbf{r}) d^3r|^2$ , where  $u_{m,\mathbf{k}}(\mathbf{r})$  is the cell-periodic part of the Bloch wave function and  $\Omega$  is the volume of the primitive cell. This overlap parameter is vital to account for the restrictions brought by the symmetries of the participating wave functions to the scattering probabilities. For the parameters of GaN, up to room temperature the thermal phonon occupation remains negligible, hence, Eq. (1) actually governs the overall scattering rate up to room temperature.

We compute the scattering rate in two alternative ways:<sup>3</sup> by direct integration over two spatial variables using the delta function or by means of the Lehmann-Taut BZ integration technique.<sup>5</sup> In the former, we prefer to work in spherical coordinates and enclose the truncated-octahedron-shaped first Brillouin zone (BZ) by a sphere of radius  $(\sqrt{5}/2)(2\pi/a)$ , where  $a$  is the lattice constant. The regions of the sphere that lie outside the first BZ are discarded by introducing a unit step function into the integrand. We em-

<sup>a)</sup>Author to whom correspondence should be addressed; present address: Department of Physics, Bilkent University, 06533 Ankara, Turkey; electronic-mail: bulutay@fen.bilkent.edu.tr

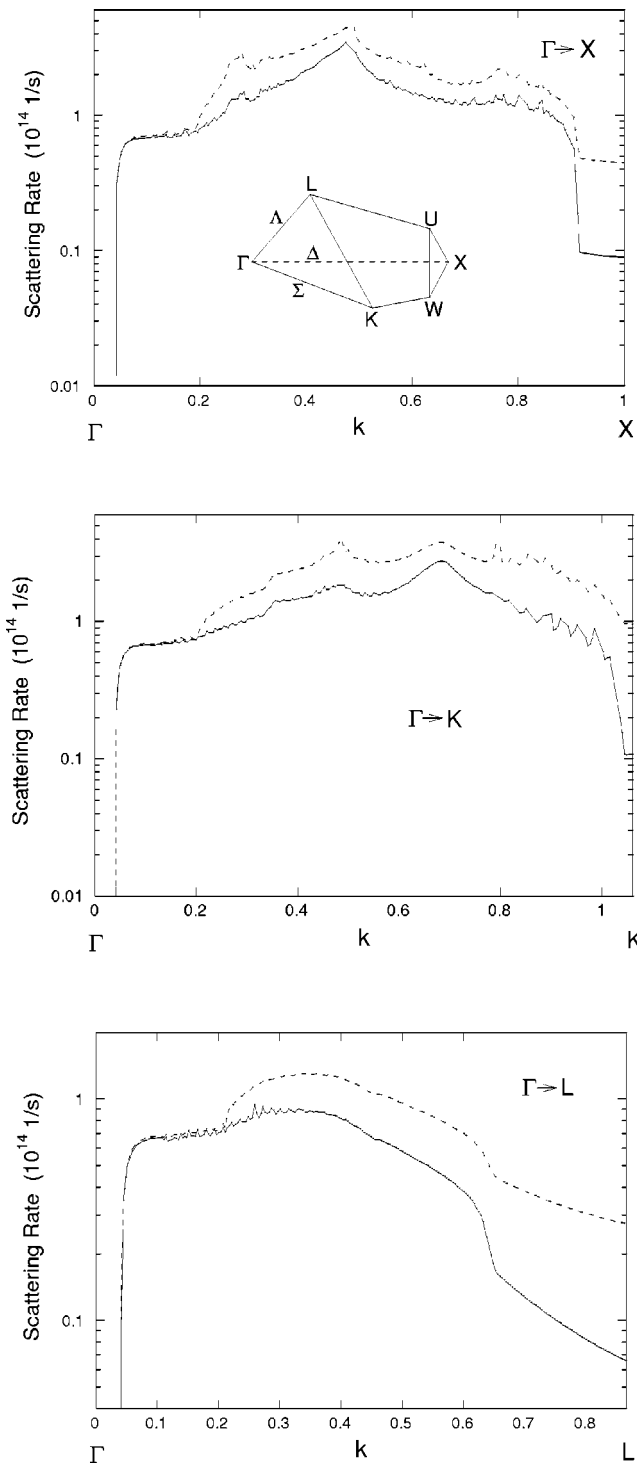


FIG. 1. POP scattering rate vs wave vector (in units of  $2\pi/a$ ) along the directions  $\Gamma$ -X,  $\Gamma$ -K, and  $\Gamma$ -L. The dashed lines indicate the same rates when the cell-periodic overlaps are taken to be unity. Inset in the upper figure shows the high-symmetry points and directions in the ZB irreducible wedge.

ploy the linear tetrahedron interpolation<sup>5</sup> of band energies and store the CB energies by sampling the irreducible wedge of the BZ by 16 114 data points, giving more emphasis to the vicinity of the  $\Gamma$  point. For the cell-periodic Bloch overlap parameter  $\Delta_{m',m}$ , we use a less dense sampling of the irreducible wedge by 1604 final-state data points for each initial electron state under consideration.

To be consistent with our previous WZ GaN analysis,<sup>3</sup> we use the following data for the cubic GaN phonons:

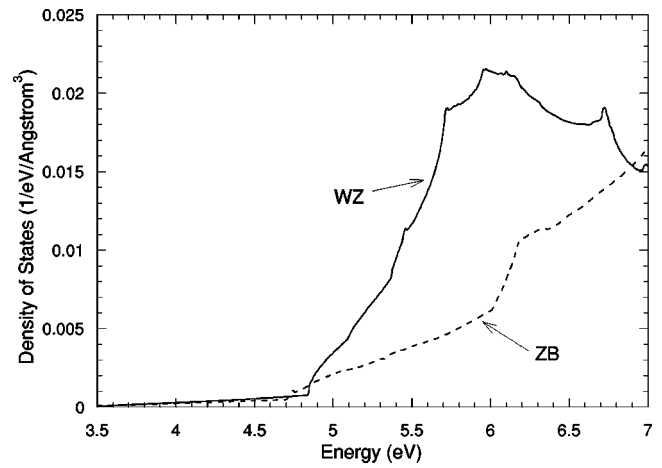


FIG. 2. Density of states per spin, per volume of the ZB (dashed) and WZ (solid) phases of GaN for the lowest conduction-band energies. The zero level of the energy is set to valence-band maximum.

$\hbar\omega_{LO}=92.12$  meV,  $\epsilon_0=9.28$ , and  $\epsilon_\infty=5.29$ . Aiming for a directional assessment, we start from the CB minimum at the  $\Gamma$  point, and trace the POP scattering rate of CB electrons along high-symmetry lines:  $\Delta$ ,  $\Sigma$ ,  $\Lambda$  corresponding to  $\Gamma$ -X,  $\Gamma$ -K, and  $\Gamma$ -L directions, respectively; see the inset in Fig. 1. The effect of setting the cell-periodic overlap parameter to unity is indicated by the dashed lines in Fig. 1 for each direction; note the resultant overestimation in the scattering rates away from the CB edge. The results indicate that the  $\Gamma$ -X ( $\Gamma$ -L) direction has the highest (lowest) scattering rate. This directional dependence can be attributed to the CB satellite valley being located at the X point, which is the major scattering destination at high energies, providing high density of final states. As the  $\Gamma$ -L direction is further away from the X valley, it requires relatively larger phonon-wave vectors, which leads to less electron-phonon coupling. Furthermore, the lowest CB along the  $\Gamma$ -L direction<sup>4</sup> does not enable an intravalley POP emission to the L point, which is the key factor behind the low scattering rate.

The  $\Gamma$ -L directions of ZB GaN are related to the  $\Gamma$ -A and  $\Gamma$ -U directions of WZ GaN.<sup>6</sup> We further note that in

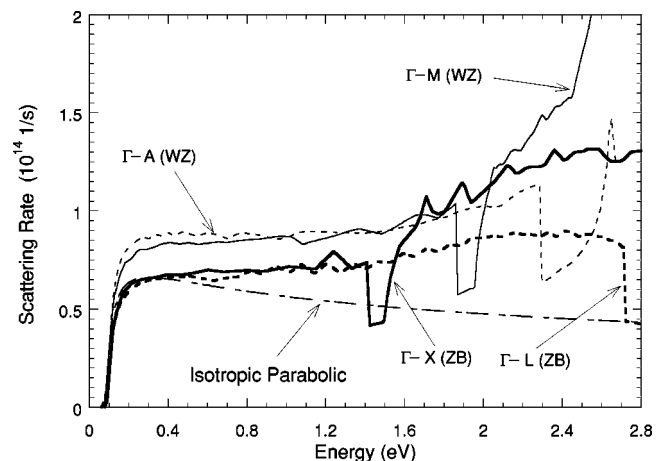


FIG. 3. POP scattering rate vs energy, comparing the ZB rates with the WZ LO-like rates along several directions. To aid comparison, for both crystal phases the energy reference is chosen to be at a same CB minimum. Cubic isotropic parabolic POP rate calculated using the CB effective mass of the ZB phase is also included.

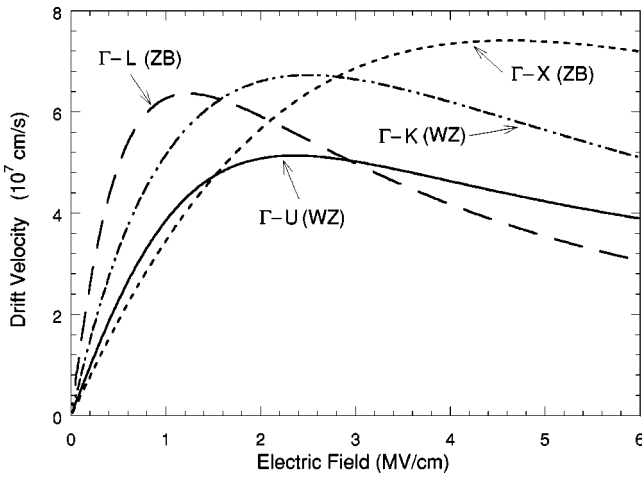


FIG. 4. Comparison of drift velocity vs electric field for the ZB and WZ phases along several directions.

WZ GaN, there exists a BZ folding along the  $c$  axis of the crystal, therefore, for the  $\Gamma$ - $A$  (WZ) direction both the lowest CB and its folded extension need to be considered.<sup>3</sup> In general terms, the ZB phase has a smaller POP scattering rate than the WZ phase, which is essentially due to the lower density of states in the former. The quantitative comparison of the density of states for these two phases around the energies relevant to our work is given in Fig. 2. However, the lower density of states in ZB GaN is shown to have one adverse consequence by leading to a lower breakdown voltage in the ZB phase due to easier heating of the CB electrons under high fields, provoking impact ionization.<sup>7</sup> The effect of the  $M$  and  $X$  satellite valleys ( $E_M = 1.87$  eV,  $E_X = 1.41$  eV above the CB edge) along the  $\Gamma$ - $M$  (WZ) and  $\Gamma$ - $X$  (ZB) directions, respectively, are seen in Fig. 3. Just at these valley energies the *average* scattering rate suddenly drops as electrons at the bottom of this valley contribute very little to the POP scattering rate, limited to intervalley scattering with large phonon-wave vectors. However, when the energy is increased further to allow the electrons in these valleys to have *intravalley* scattering, the rate rapidly rises. The isotropic-parabolic band estimation for the POP rate is also shown to illustrate the validity range of this approximation as compared to a full-band treatment; only up to  $\sim 0.4$  eV above the CB edge there is seen to be a good agreement.

Following Esaki and Tsu's phenomenological semiclassical treatment,<sup>8</sup> we estimate the drift velocity dependence on the electric field. Accordingly, the average drift velocity assuming a constant scattering time  $\tau$  is given by

$$v_d = eF\hbar^{-2} \int_0^\infty \frac{\partial^2 E_{\text{Fld}}}{\partial k_{\text{Fld}}^2} e^{-t/\tau} dt, \quad (2)$$

where  $\partial^2 E_{\text{Fld}} / \partial k_{\text{Fld}}^2$  is the curvature of the energy-band diagram along the applied field's direction  $\mathbf{F}$ , sampled at the  $\mathbf{k}$  point,  $k_{\text{Fld}}(t) = eFt/\hbar$ , for an electron originating from the  $\Gamma$  point. For the scattering time  $\tau$  in Eq. (2), we use the value given by the *maximum* scattering rate in each direction. Figure 4 shows the corresponding drift velocity estimations relevant to *high* fields for both crystal phases. Different low-

field mobilities in Fig. 4, contrary to reality, are caused by using the maximum scattering rate throughout the band, even though this rate shows an isotropic character close to the CB edge (cf. Fig. 1). The  $\Gamma$ - $L$  direction of ZB GaN has the lowest onset field of 1 MV/cm for the observation of negative differential conductivity (NDC), however, note the sensitivity of the onset field to angular variations (cf. Fig. 4). There have already been several predictions of NDC in GaN (Refs. 9–12) at field levels of around 150 kV/cm, all being based on the transfer of electrons to upper valleys, whereas, the NDC that we refer to here is caused by those carriers reaching the negative effective mass part of the band structure at high fields before undergoing a scattering event, an idea initially proposed by Krömer.<sup>13</sup> Recently, the possibility of NDC based on this mechanism was advocated<sup>14</sup> for cubic GaN beyond a field of  $\sim 50$  kV/cm. This onset voltage is about 20 times lower than our estimate. Recent Monte Carlo investigations<sup>15</sup> along this line did not encounter any drastic change up to fields  $\sim 0.5$  MV/cm with respect to a variation of the energy of the  $X$  valley, which further contradicts this previous prediction.<sup>14</sup>

In summary, to aid the high-field characterization of GaN, we present a full-band POP scattering analysis of CB electrons, comparing the ZB and WZ crystal phases. In general, the scattering rates in the ZB phase are lower than the WZ phase due to the lower density of states in the former. This suggests a possibility to have enhanced *high-field* mobility in ZB GaN in comparison with WZ GaN. High-field transport along the  $\Gamma$ - $L$  direction of ZB GaN characterized by a scattering time of 11 fs has the lowest scattering rate, as the POP emission to the  $L$  point is energetically not possible. The observation of NDC driven by the negative effective mass part of the band structure is predicted beyond a field of roughly 1 MV/cm for the ZB phase, and 2.3 MV/cm for the WZ phase.

This work is supported by ONR (Contract No. N00014-99-1-0014) and EPSRC (Contract No. GR/L/56725).

<sup>1</sup>J. W. Orton and C. T. Foxon, Rep. Prog. Phys. **61**, 1 (1998).

<sup>2</sup>A. García and M. L. Cohen, Phys. Rev. B **47**, 4215 (1993); **47**, 4221 (1993).

<sup>3</sup>C. Bulutay, B. K. Ridley, and N. A. Zakhleniuk, Phys. Rev. B (in press).

<sup>4</sup>R. Wang, P. P. Ruden, J. Kolnik, I. Oğuzman, and K. F. Brennan, J. Phys. Chem. Solids **58**, 913 (1997).

<sup>5</sup>G. Lehmann and M. Taut, Phys. Status Solidi B **54**, 469 (1972).

<sup>6</sup>M. R. Salehpour and S. Satpathy, Phys. Rev. B **41**, 3048 (1990).

<sup>7</sup>M. Farahmand and K. F. Brennan, IEEE Trans. Electron Devices **47**, 493 (2000).

<sup>8</sup>L. Esaki and R. Tsu, IBM J. Res. Dev. **14**, 61 (1970).

<sup>9</sup>B. Gelmont, K. Kim, and M. Shur, J. Appl. Phys. **74**, 1818 (1993).

<sup>10</sup>N. S. Mansour, K. W. Kim, and M. A. Littejohn, J. Appl. Phys. **77**, 2834 (1995).

<sup>11</sup>J. Kolnik, İ. H. Oğuzman, K. F. Brennan, R. Wang, P. P. Ruden, and Y. Wang, J. Appl. Phys. **78**, 1033 (1995).

<sup>12</sup>B. E. Foutz, S. K. O'Leary, M. S. Shur, and L. F. Eastman, J. Appl. Phys. **85**, 7727 (1999).

<sup>13</sup>H. Krömer, Phys. Rev. **109**, 1856 (1958).

<sup>14</sup>S. Krishnamurthy, M. van Schilfgaarde, A. Sher, and A.-B. Chen, Appl. Phys. Lett. **71**, 1999 (1997).

<sup>15</sup>K. F. Brennan (private communication).